Available online at www.sciencedirect.com
ScienceDirect
Journal of Sound and Vibration 313 (2008) 205–223
JOURNAL OF SOUND AND VIBRATION
www.elsevier.com/locate/jsvi

Free vibration analysis of laminated plate/shell structures based on FSDT with a stabilized nodal-integrated quadrilateral element

H. Nguyen-Van, N. Mai-Duy, T. Tran-Cong*

Faculty of Engineering and Surveying, Computational Engineering & Science Research Centre (CESRC), University of Southern Queensland, Toowoomba, QLD 4350, Australia

Received 19 September 2007; received in revised form 16 November 2007; accepted 17 November 2007
Available online 9 January 2008

Abstract

This paper reports numerical analyses of free vibration of laminated composite plate/shell structures of various shapes, span-to-thickness ratios, boundary conditions and lay-up sequences. The method is based on a novel four-node quadrilateral element, namely MISQ20, within the framework of the first-order shear deformation theory (FSDT). The element is built by incorporating a strain smoothing method into the bilinear four-node quadrilateral finite element where the strain smoothing operation is based on mesh-free conforming nodal integration. The bending and membrane stiffness matrices are based on the boundaries of smoothing cells while the shear term is evaluated by 2×2 Gauss quadrature. Through several numerical examples, the capability, efficiency and simplicity of the element are demonstrated. Convergence studies and comparison with other existing solutions in the literature suggest that the present element is robust, computationally inexpensive and free of locking.

1. Introduction

The analysis of natural frequencies of composite plates/shells plays an increasingly important role in the design of structures in mechanical, civil and aerospace engineering applications. A thorough study of the dynamic behaviors of these structures is essential in assessing their full potential. Therefore, it is necessary to develop appropriate models capable of accurately predicting their dynamic characteristics.

Great progress has been made over past decades towards better understanding of the vibration characteristics of laminated composite plates/shells [1–3]. Due to limited availability of analytic solutions for practical applications, numerical approximate methods have become the most effective tools. The finite element method (FEM) is considered to be a very effective and versatile approach for these problems. There is a vast amount of literature on free vibration analysis of laminated plates/shells which is too large to list here. Bert [1] and Mohamad [2] have conducted surveys and provided details on the development of the FEMs for

*Corresponding author. Tel.: +61 7 46312539; fax: +61 7 46312526.
E-mail address: trancong@usq.edu.au (T. Tran-Cong).

0022-460X/$ - see front matter © 2007 Elsevier Ltd. All rights reserved.
doi:10.1016/j.jsv.2007.11.043

modeling and modal analysis of laminated plates/shells. Further extensive references on shells can be found in the excellent review of Yang et al. [3].

Although the FEM solution is quite effective and versatile, its performance is highly mesh dependent and badly deteriorates when mesh distortion occurs. On the other hand, the mesh-free methods have become an alternative approach for problems with complex geometry and boundary conditions. Several mesh-free methods have been so far proposed for vibration analysis, including the element free Galerkin (EFG) method [4], the moving least square differential quadrature (MLSDQ) method [5,6], the radial basis function (RBF) method [7,8] and the reproducing Kernel particle method [9], etc. However, the complex approximation space of mesh-fee methods increases the computational cost of solving the resultant algebraic equation systems. Recently, Liu et al. [10,11] proposed a new smoothed finite element method (SFEM) where the strain smoothing technique of the stabilized conforming nodal integration (SCNI) mesh-free method was incorporated into the existing FEM for 2D elastic problems. Based on the idea of SFEM, Nguyen-Van et al. [12] have developed a new locking-free quadrilateral laminated plate element MISQ20 by incorporating the SCNI into the Bathe-Dvorkin assumed strain plate element [13]. It is found that the MISQ20 element with SCNI is effective, computationally inexpensive and not sensitive to mesh distortion. It is able to achieve accurate results even with coarse discretization irrespective of the span-to-thickness ratio and stacking sequence.

The goal of the present study is to extend the MISQ20 element for analysis of free vibration problems of laminated plate/shell structures within the framework of the FSDT. Eigenvalue analysis of various composite plates/shells is performed in order to have a better understanding of their dynamic behaviors associated with different parameters such as boundary conditions, types of laminates, mesh distortion, fiber orientation, span-to-thickness ratio, mixed boundaries and modulus ratio.

The paper is outlined as follows. First, a brief review of the finite element formulations for laminated plates is introduced in Section 2. The description of strain smoothing technique for FEM is derived in Section 3. Several numerical investigations are carried out in Section 4 to assess the performance of the proposed element in free vibration analysis. Finally, concluding remarks are made in Section 5.

2. Finite element formulations for laminated plates

In the first-order shear deformation theory (FSDT) [14], the plate kinematics is governed by the midplane displacement u_o, v_o, w_o and rotation θ_x, θ_y as follows:

$$u(x,y,z) = u_o(x,y) + z\theta_x,$$

$$v(x,y,z) = v_o(x,y) + z\theta_y,$$

$$w(x,y,z) = w_o(x,y). \tag{1}$$

A typical four-node quadrilateral laminated plate element consisting of n layers with thickness h is shown in Fig. 1.

The in-plane strain vector $\boldsymbol{\varepsilon} = [\varepsilon_x \ \ \varepsilon_y \ \ \varepsilon_{xy}]^{\mathrm{T}}$ can be rewritten as

$$\boldsymbol{\varepsilon} = \begin{bmatrix} u_{o,x} \\ v_{o,y} \\ u_{o,y} + v_{o,x} \end{bmatrix} + z \begin{bmatrix} \theta_{x,x} \\ \theta_{y,y} \\ \theta_{x,y} + \theta_{y,x} \end{bmatrix} = \boldsymbol{\varepsilon}_m + z\boldsymbol{\varepsilon}_b \tag{2}$$

and the transverse shear strain vector as

$$\boldsymbol{\gamma} = [\gamma_{xz} \ \ \gamma_{yz}]^{\mathrm{T}} = [\theta_x - w_{,x} \ \ \theta_y - w_{,y}]^{\mathrm{T}}. \tag{3}$$

For an anisotropic laminated plate, the stress and resultant constitutive relationship are expressed as follows:

$$\boldsymbol{\sigma}_p = \begin{Bmatrix} \mathbf{N} \\ \mathbf{M} \end{Bmatrix} = \begin{bmatrix} \mathbf{A} & \mathbf{B} \\ \mathbf{B} & \mathbf{D} \end{bmatrix} \begin{Bmatrix} \boldsymbol{\varepsilon}_m \\ \boldsymbol{\varepsilon}_b \end{Bmatrix} = \mathbf{C}_p \boldsymbol{\varepsilon}_p, \tag{4}$$

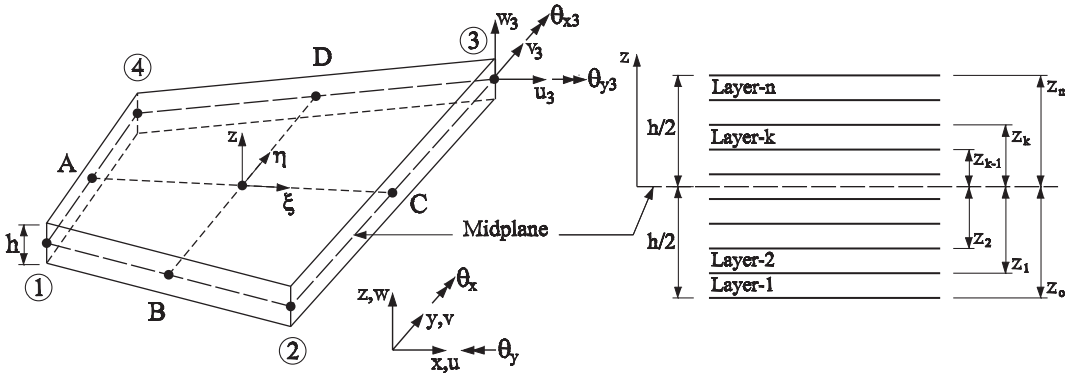

Fig. 1. A quadrilateral laminated plate element consisting of n layers.

$$\mathbf{T} = \begin{bmatrix} k_1^2 \bar{C}_{55}^0 & k_1 k_2 \bar{C}_{45}^0 \\ k_1 k_2 \bar{C}_{45}^0 & k_2^2 \bar{C}_{44}^0 \end{bmatrix} \begin{Bmatrix} \gamma_{xz} \\ \gamma_{yz} \end{Bmatrix} = \mathbf{C}_s \boldsymbol{\gamma}, \tag{5}$$

where $\mathbf{N} = [N_x \ N_y \ N_{xy}]^{\mathrm{T}}$, $\mathbf{M} = [M_x \ M_y \ M_{xy}]^{\mathrm{T}}$, $\mathbf{T} = [Q_x \ Q_y]^{\mathrm{T}}$ are the membrane force vector, the bending moment vector and the transverse shear force vector, respectively; k_1^2, k_2^2 are shear correction factors (SCFs) which can be estimated by using special methods [15–17]; **A**, **B**, **D**, **C** are matrices of extensional stiffness, bending–extensional coupling stiffness, bending stiffness and transverse shearing stiffness, respectively, defined as

$$(A_{ij}, B_{ij}, D_{ij}) = \int_{-h/2}^{h/2} (1, z, z^2) \bar{Q}_{ij} \, \mathrm{d}z, \quad i,j = 1,2,6,$$

$$C_{ij}^0 = \int_{-h/2}^{h/2} \bar{Q}_{ij} \, \mathrm{d}z, \quad i,j = 4,5, \tag{6}$$

where $\bar{Q}_{ij}$ are the elastic constants with respect to the global x-axis and their detailed definitions can be found in Ref. [14].

Base on the FSDT, the finite element solution $\mathbf{u}$ of a displacement model for laminated plates is approximated as

$$\mathbf{u} = \begin{Bmatrix} u \\ v \\ w \\ \theta_x \\ \theta_y \end{Bmatrix} = \sum_{i=1}^{np} \begin{bmatrix} N_i & 0 & 0 & 0 & 0 \\ 0 & N_i & 0 & 0 & 0 \\ 0 & 0 & N_i & 0 & 0 \\ 0 & 0 & 0 & N_i & 0 \\ 0 & 0 & 0 & 0 & N_i \end{bmatrix} \mathbf{q}_i, \tag{7}$$

where np ($np = 4$ in this case) is the total number of nodes of an element, $\mathbf{q}_i = [u_i \ v_i \ w_i \ \theta_{xi} \ \theta_{yi}]^{\mathrm{T}}$ is the nodal displacement vector and $N_i = \frac{1}{4}(1 + \xi_i \xi)(1 + \eta_i \eta)$ is the shape function of the four-node serendipity element.

The corresponding approximation of membrane, bending and shear strain of Eq. (4) can be expressed in the following form:

$$\boldsymbol{\varepsilon}_p = \begin{Bmatrix} \boldsymbol{\varepsilon}_m \\ \boldsymbol{\varepsilon}_b \end{Bmatrix} = \begin{bmatrix} \mathbf{B}_m \\ \mathbf{B}_b \end{bmatrix} \mathbf{q} = \mathbf{B}_p \mathbf{q}, \tag{8}$$

$$\boldsymbol{\gamma} = \begin{Bmatrix} \gamma_{xz} \\ \gamma_{yz} \end{Bmatrix} = \mathbf{B}_s \mathbf{q}, \tag{9}$$

$$\mathbf{B}_m = \begin{pmatrix} N_{i,x} & 0 & 0 & 0 & 0 \\ 0 & N_{i,y} & 0 & 0 & 0 \\ N_{i,y} & N_{i,x} & 0 & 0 & 0 \end{pmatrix}, \quad \mathbf{B}_b = \begin{pmatrix} 0 & 0 & 0 & N_{i,x} & 0 \\ 0 & 0 & 0 & 0 & N_{i,y} \\ 0 & 0 & 0 & N_{i,y} & N_{i,x} \end{pmatrix}, \tag{10}$$

$$\mathbf{B}_s = \begin{pmatrix} 0 & 0 & N_{i,x} & N_i & 0 \\ 0 & 0 & N_{i,y} & 0 & N_i \end{pmatrix}. \tag{11}$$

The element stiffness matrix can be written based on the minimum potential principle as

$$\mathbf{K}^e = \mathbf{K}^e_{mb} + \mathbf{K}^e_s = \int_{\Omega^e} \mathbf{B}_p^{\mathrm{T}} \mathbf{C}_p \mathbf{B}_p \, \mathrm{d}\Omega + \int_{\Omega^e} \mathbf{B}_s^{\mathrm{T}} \mathbf{C}_s \mathbf{B}_s \, \mathrm{d}\Omega. \tag{12}$$

By using Hamilton's principle, the equation of motion of an element can be obtained as

$$\mathbf{M}^e \ddot{\mathbf{q}} + \mathbf{K}^e \mathbf{q} = 0, \tag{13}$$

which leads to the following eigenvalue equation:

$$(\mathbf{K}^e - \omega^2 \mathbf{M}^e)\mathbf{q} = 0, \tag{14}$$

where the element mass matrix is defined by

$$\mathbf{M}^e = \int_{\Omega^e} \mathbf{N}_m^{\mathrm{T}} \mathbf{m} \mathbf{N}_m \, \mathrm{d}\Omega, \tag{15}$$

in which

$$\mathbf{N}_m = \begin{bmatrix} N_i & 0 & 0 & 0 & 0 \\ 0 & N_i & 0 & 0 & 0 \\ 0 & 0 & N_i & 0 & 0 \\ 0 & 0 & 0 & N_i & 0 \\ 0 & 0 & 0 & 0 & N_i \end{bmatrix}, \quad \mathbf{m} = \rho h \begin{bmatrix} 1 & 0 & 0 & 0 & 0 \\ 0 & 1 & 0 & 0 & 0 \\ 0 & 0 & 1 & 0 & 0 \\ 0 & 0 & 0 & \dfrac{h^2}{12} & 0 \\ 0 & 0 & 0 & 0 & \dfrac{h^2}{12} \end{bmatrix}. \tag{16}$$

3. Strain smoothing approach for finite element method

3.1. Smoothed membrane-bending strain approximation

The membrane-bending strains at an arbitrary point $\mathbf{x}_C$ can be obtained by using following strain smoothing operation:

$$\tilde{\boldsymbol{\varepsilon}}_p(\mathbf{x}_C) = \int_{\Omega_C} \boldsymbol{\varepsilon}_p(\mathbf{x}) \Phi(\mathbf{x} - \mathbf{x}_C) \, \mathrm{d}\Omega, \tag{17}$$

where $\boldsymbol{\varepsilon}_p$ is the membrane-bending strain obtained from displacement compatibility condition as given in Eq. (8); Ω_C is the smoothing cell domain on which the smoothing operation is performed (Ω_C may be an entire element or part of an element as shown in Fig. 2, depending on the stability analysis [10,11]); Φ is a given smoothing function that satisfies at least unity property $\int_{\Omega_C} \Phi \, \mathrm{d}\Omega = 1$ and is defined as

$$\Phi(\mathbf{x} - \mathbf{x}_C) = \begin{cases} 1/A_C, & \mathbf{x} \in \Omega_C, \\ 0, & \mathbf{x} \notin \Omega_C, \end{cases} \tag{18}$$

in which $A_C = \int_{\Omega_C} \mathrm{d}\Omega$ is the area of the smoothing cell (subcell).

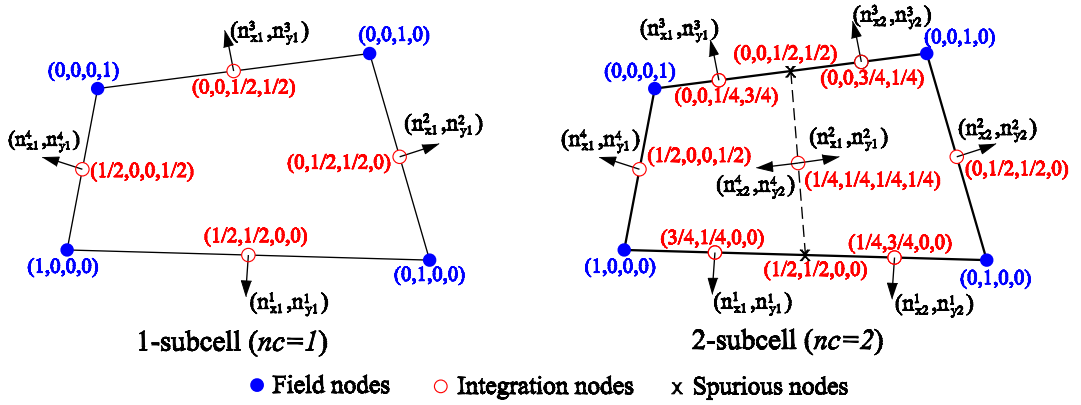

Fig. 2. Subdivision of an element into smoothing cells (nc) and the values of shape functions at nodes.

Substituting Φ into Eq. (17) and applying the divergence theorem, one can get a smoothed membrane-bending strains as

$$\tilde{\boldsymbol{\varepsilon}}_p(\mathbf{x}_C) = \begin{Bmatrix} \tilde{\boldsymbol{\varepsilon}}_m(\mathbf{x}_C) \\ \tilde{\boldsymbol{\varepsilon}}_b(\mathbf{x}_C) \end{Bmatrix} = \frac{1}{2A_C} \begin{Bmatrix} \int_{\Gamma_C} (u_i n_j + u_j n_i)\,\mathrm{d}\Gamma \\ \int_{\Gamma_C} (\theta_i n_j + \theta_j n_i)\,\mathrm{d}\Gamma \end{Bmatrix}, \tag{19}$$

where Γ_C is the boundary of the smoothing cell.

Introducing the finite element approximation of $\mathbf{u}$ into Eq. (7) gives

$$\tilde{\boldsymbol{\varepsilon}}_p(\mathbf{x}_C) = \sum_{i=1}^{nc} [\tilde{\mathbf{B}}_{mi}(\mathbf{x}_C) \;\; \tilde{\mathbf{B}}_{bi}(\mathbf{x}_C)]^{\mathrm{T}} \mathbf{q}_i = \sum_{C=1}^{nc} \tilde{\mathbf{B}}_p^C(\mathbf{x}_C)\mathbf{q}, \tag{20}$$

where

$$\tilde{\mathbf{B}}_{pi}^C(\mathbf{x}_C) = \frac{1}{A_C} \int_{\Gamma_C} \begin{pmatrix} N_i n_x & 0 & 0 & 0 & 0 \\ 0 & N_i n_y & 0 & 0 & 0 \\ N_i n_y & N_i n_x & 0 & 0 & 0 \\ 0 & 0 & 0 & N_i n_x & 0 \\ 0 & 0 & 0 & 0 & N_i n_y \\ 0 & 0 & 0 & N_i n_y & N_i n_x \end{pmatrix} \mathrm{d}\Gamma. \tag{21}$$

If one Gaussian point is used to evaluate Eq. (21) along each line segment of the boundary Γ_i^C of Ω_C, Eq. (21) can be transformed as follows:

$$\tilde{\mathbf{B}}_{pi}^C(\mathbf{x}_C) = \frac{1}{A_C} \sum_{b=1}^{nb} N_i(\mathbf{x}_b^G) \begin{pmatrix} n_x & 0 & 0 & 0 & 0 \\ 0 & n_y & 0 & 0 & 0 \\ n_y & n_x & 0 & 0 & 0 \\ 0 & 0 & 0 & n_x & 0 \\ 0 & 0 & 0 & 0 & n_y \\ 0 & 0 & 0 & n_y & n_x \end{pmatrix} l_b^C, \tag{22}$$

where x_b^G and l_b^C are the midpoint (Gauss point) and the length of Γ_b^C, respectively, and nb is the total number of edges of each smoothing cell.

3.2. Transverse shear strains of the element

The shear strains are approximated with independent interpolation fields in the natural coordinate system [13] as

$$\begin{bmatrix}\gamma_x\\ \gamma_y\end{bmatrix} = \mathbf{J}^{-1}\begin{bmatrix}\gamma_\xi\\ \gamma_\eta\end{bmatrix} = \mathbf{J}^{-1}\hat{\mathbf{N}}\begin{bmatrix}\gamma_\eta^A\\ \gamma_\xi^B\\ \gamma_\eta^C\\ \gamma_\xi^D\end{bmatrix}, \tag{23}$$

in which

$$\hat{\mathbf{N}} = \frac{1}{2}\begin{bmatrix}(1-\xi) & 0 & (1+\xi) & 0\\ 0 & (1-\eta) & 0 & (1+\eta)\end{bmatrix}, \tag{24}$$

$\mathbf{J}$ is the Jacobian matrix and the midside nodes A, B, C, D are shown in Fig. 1. Expressing γ_η^A, γ_η^C and γ_ξ^B, γ_ξ^D in terms of the discretized fields $\mathbf{u}$, we obtain the shear matrix

$$\bar{\mathbf{B}}_{si} = \mathbf{J}^{-1}\begin{bmatrix}0 & 0 & N_{i,\xi} & -b_i^{12}N_{i,\xi} & b_i^{11}N_{i,\xi}\\ 0 & 0 & N_{i,\eta} & -b_i^{22}N_{i,\eta} & b_i^{21}N_{i,\eta}\end{bmatrix}, \tag{25}$$

where

$$b_i^{11} = \xi_i x_{,\xi}^M, \quad b_i^{12} = \xi_i y_{,\xi}^M, \quad b_i^{21} = \eta_i x_{,\eta}^L, \quad b_i^{22} = \eta_i y_{,\eta}^L, \tag{26}$$

in which $\xi_i \in \{-1,1,1,-1\}, \eta_i \in \{-1,-1,1,1\}$ and $(i,M,L) \in \{(1,B,A);(2,B,C);(3,D,C);(4,D,A)\}$. The element stiffness matrix in Eq. (12) can be transformed as follows:

$$\tilde{\mathbf{K}}^e = \tilde{\mathbf{K}}_{mb}^e + \bar{\mathbf{K}}_s^e = \sum_{C=1}^{nc}\tilde{\mathbf{B}}_{pC}^{\mathrm{T}}\mathbf{C}_p\tilde{\mathbf{B}}_{pC}A_C + \int_{\Omega_e}\bar{\mathbf{B}}_s^{\mathrm{T}}\mathbf{C}_s\bar{\mathbf{B}}_s\,\mathrm{d}\Omega. \tag{27}$$

Finally, the linear equation of motion in Eq. (14) can be rewritten as

$$(\tilde{\mathbf{K}}^e - \omega^2\mathbf{M}^e)\mathbf{q} = 0, \tag{28}$$

In Eq. (27), the shear term $\bar{\mathbf{K}}_s^e$ is still computed by 2×2 Gauss quadrature while the element bending stiffness $\tilde{\mathbf{K}}_{mb}^e$ is computed by one Gaussian point along each line segment of the smoothing cells of the element. For simplicity, two smoothing cells ($nc = 2$) as shown in Fig. 2 are used for calculating the smoothed membrane-bending stiffness matrix of the element. This forms the basis of a new four-node quadrilateral element named MISQ20 (mixed interpolation smoothing quadrilateral element with 20 degree-of-freedom, dof) for analysis of laminated plates. For analysis of laminated shells using MISQ20 flat element, a drilling dof θ_z (inplane rotation) will be added to each node for assembling the stiffness matrices and the total dofs will be 24. To avoid rank deficiency of the element stiffness matrix, the fictitious stiffness associated with the drilling dof is taken to be equal to $1/1000$ of the maximum diagonal value of the element stiffness matrix.

4. Numerical results and discussions

In this section, a number of numerical examples are presented to demonstrate the performance of the MISQ20 element in the analysis of free vibration of laminated plates/shells. Particular plate/shell structures with various boundary conditions, span-to-thickness ratios and modulus ratios (the degree of orthotropy) are analyzed. In all examples, the material properties are assumed to be the same in all the layers and the fiber orientations may be different among the layers. The ply angle of each layer is measured from the global x-axis to the fiber direction. All layers have the same thickness and the mass density ρ is taken to be uniform in the thickness direction. Unless otherwise specified, SCFs $k_1^2 = k_2^2 = \pi^2/12$ are used for all computations.

The following material parameters of a layer are used in all plate examples $E_1/E_2 = 10$, 20, 30 or 40; $G_{12} = G_{13} = 0.6E_2$; $G_{23} = 0.5E_2$; $v_{12} = v_{13} = v_{23} = 0.25$; $\rho = 1$.

4.1. Square laminated plates

This section deals with cross-ply laminated square plates with various span-to-thickness ratios, number of layers, boundary conditions and lay-up stacking sequences. A typical representative sketch of a mesh of 14×14 used in these analyses is shown in Fig. 3.

4.1.1. Convergence study and the effect of modulus ratios

A simply supported four-layer cross-ply [0/90/90/0] square laminated plate is chosen to study the convergence of the present method using MISQ20 element. The span-to-thickness ratio of the plate a/h is taken to be 5 in the computation. Table 1 shows the convergence and comparison of the normalized fundamental frequencies of the present method with other solutions for various degrees of orthotropy of the individual layers (E_1/E_2 ratio). It is found that the MISQ20 element yields not only relatively accurate results in a wide range of E_1 to E_2 ratios but also rapid convergence as shown in Fig. 4a. The effect of various modulus ratios of E_1/E_2 on the accuracy of the fundamental frequency is also displayed in Fig. 4b. It can be seen that the present results are in good agreement with exact solutions [14,18] and closer to MLSDQ's solutions by Liew et al. [5] than RBF's results of Ferreira et al. [7].

4.1.2. Mesh distortion

The influence of mesh distortion is studied in this section. The plate of the first example (Section 4.1.1) is analyzed again using distorted element created by irregular interior nodes. These interior nodes are derived

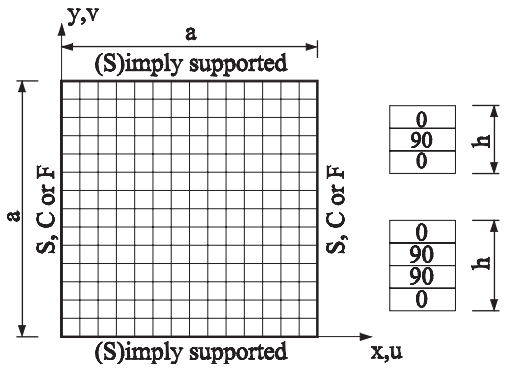

Fig. 3. Geometry and discretization of square laminated plates.

Table 1
Simply supported cross-ply [0/90/90/0] square plate: convergence of normalized fundamental frequencies and comparison with other solutions ($\omega^* = (\omega a^2/h)\sqrt{\rho/E_2}$, $a/h = 5$)

Model	Mesh	E_1/E_2			
		10	20	30	40
MISQ20	6×6	8.4443	9.7149	10.4729	11.0001
	10×10	8.3384	9.6010	10.3548	10.8792
	12×12	8.3203	9.5815	10.3346	10.8585
	14×14	8.3094	9.5698	10.3224	10.8471
MLSDQ [5]		8.2924	9.5613	10.320	10.849
RBF [7]		8.3101	9.5801	10.349	10.864
Exact [18,14]		8.2982	9.5671	10.326	10.854

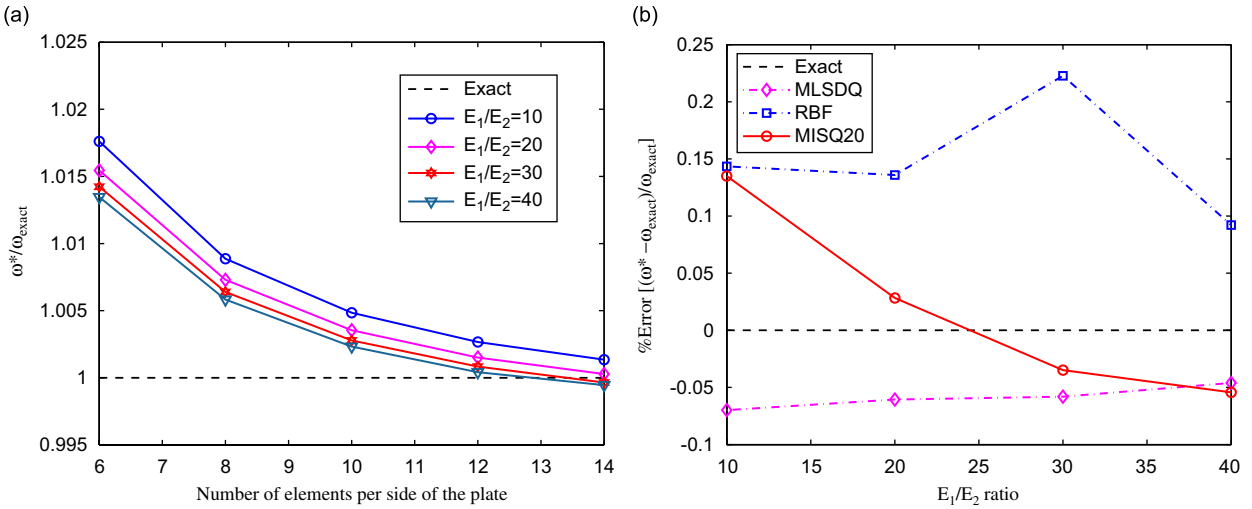

Fig. 4. Square cross-ply [0/90/90/0] laminated plate: (a) convergence of the present method and (b) effect of modulus ratios on the accuracy of fundamental frequencies.

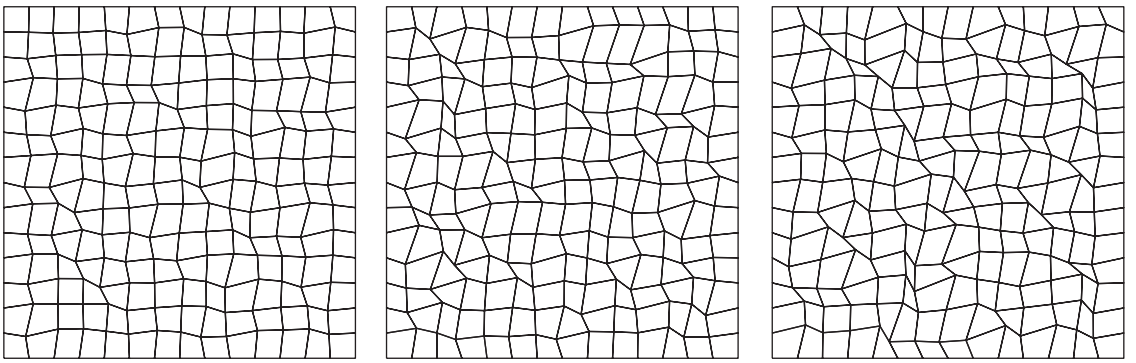

Fig. 5. Typical irregular meshes with various distortion factor s.

from a set of regular nodes by using a controlling distortion factor s. Thus, the coordinates of an irregular mesh are obtained by the following expressions:

$$x' = x + r_c s \Delta x,$$

$$y' = y + r_c s \Delta y, \tag{29}$$

where r_c is a computer-generated random number between -1.0 and 1.0, $\Delta x, \Delta y$ are initial regular element sizes in the x- and y-directions, respectively and $s \in [0, 0.4]$ is used to control the shapes of the distorted elements: the bigger value of s, the more irregular the shape of generated elements. Typical irregular meshes of the analysis are shown in Fig. 5.

The effect of the mesh distortion on the fundamental frequency of the plate obtained by the present method is shown in Table 2 and Fig. 6. It is found that the accuracy of the fundamental frequencies associated with irregular mesh decreases in comparison with regular meshes. However, the deterioration is very small and the overall performance is insensitive to mesh distortion as the maximum error of frequency is below 0.3% (in the case of $E_1/E_2 = 10$). For the cases of $E_1/E_2 = 30$ and 40, Fig. 6 indicates that the error at some s could become even smaller than those at $s = 0$ (regular mesh).

Table 2
Simply supported cross-ply [0/90/90/0] square plate: effect of mesh distortion on the normalized fundamental frequencies ($\omega^* = (\omega a^2/h)\sqrt{\rho/E_2}$, $a/h = 5$)

E_1/E_2	$s = 0$	$s = 0.1$	$s = 0.2$	$s = 0.3$	$s = 0.4$
40	10.8471	10.8476	10.8495	10.8528	10.8597
30	10.3224	10.3239	10.3257	10.3283	10.3354
20	9.5698	9.5712	9.5728	9.5749	9.5820
10	8.3094	8.3108	8.3125	8.3140	8.3207

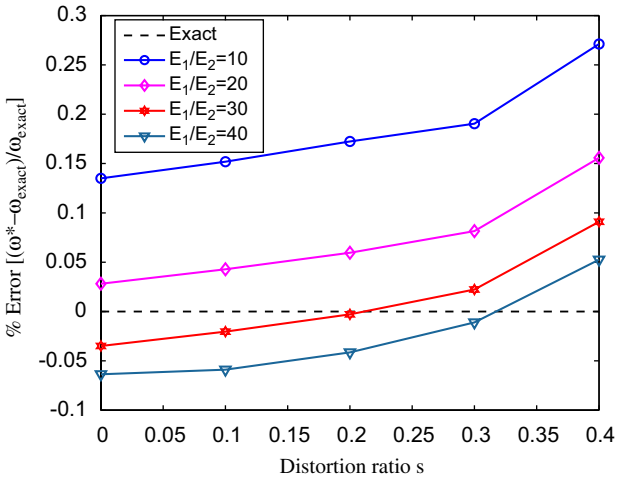

Fig. 6. Square cross-ply [0/90/90/0] laminated plate: effect of mesh distortion on the accuracy of the fundamental frequency.

Table 3
Simply supported cross-ply [0/90/90/0] square plate with various a/h ratios: convergence of normalized fundamental frequencies and comparison with other solutions ($\omega^* = (\omega a^2/h)\sqrt{\rho/E_2}$, $E_1/E_2 = 40$)

Model		a/h					
		5	10	20	25	50	100
MISQ20	6×6	11.0001	15.4187	18.0504	18.4839	19.1221	19.2939
	10×10	10.8792	15.2201	17.7903	18.2122	18.8325	18.9992
	14×14	10.8461	15.1658	17.7192	18.1380	18.7535	18.9189
p-Ritz [20]		10.8550	15.1434	17.6583	18.0718	18.6734	18.8359
RBF-pseudospectral [8]		10.8074	15.1007	17.6338	18.0490	18.6586	18.8223
Reddy and Phan [19]		10.9891	15.2689	17.6669	18.0490	18.4624	18.7561
Cho et al. [23]		10.673	15.066	17.535	18.054	18.670	18.835
Local theory [21]		10.682	15.069	17.636	18.055	18.670	18.835
Global theory [22]		10.6876	15.0721	17.6369	18.0557	18.6702	18.8352
Global-local theory [24]		10.7294	15.1658	17.8035	18.2404	18.9022	19.1566

4.1.3. *Effect of span-to-thickness ratio*

This section deals with the effect of the span-to-thickness ratio (a/h) on the fundamental frequency of a simply supported square cross-ply plate made of material having $E_1/E_2 = 40$. Table 3 presents a convergence study on the normalized fundamental frequency. The present numerical results are comparable with those of Reddy and Phan [19] who used higher-order shear deformation theory, Liew [20] who used a *p*-Ritz solution, Wu et al. [21] who used local higher-order theory, Matsunaga [22] who used global higher-order theory, Striz

et al. [23] who used higher-order individual-layer theory and Zhen et al. [24] who used global–local higher-order theory. However, it can be seen that the present results are in closer agreement with results of Liew than other methods cited here. From Table 3, it is also noticed that the span-to-thickness ratio has a considerable effect on the fundamental frequency of plates at lower a/h ratios. At higher a/h ratios ($a/h > 25$), the influence on the fundamental frequency is minor.

4.1.4. *Effect of lay-up sequence and fiber orientation*

To investigate the effect of lay-up sequence and fiber orientation, this section reports the analysis of two composite plates with lamination sequence $[\theta/0/0/\theta]$ and $[0/\theta/\theta/0]$ with simply supported (SSSS) and clamped (CCCC) edges. The span-to-thickness ratio of the plate $a/h = 100$ and modulus ratio $E_1/E_2 = 10$ are used in the computation. Fig. 7 shows the effects of both fiber orientation and lay-up sequence on the fundamental frequencies. It is found that there is symmetry for the orientation angle of 45° in both cases of simply supported and clamped conditions. Moreover, in the case of SSSS edge conditions, the $[\theta/0/0/\theta]$ lamination results in a higher fundamental frequencies than the corresponding ones for the $[0/\theta/\theta/0]$ sequence. In the case of CCCC edge conditions, the behavior of the fundamental frequencies is opposite to the above SSSS results. It appears that, in both cases, the fundamental frequencies has an extremum at ply angle $\theta = 45°$.

4.1.5. *Influence of mixed boundaries and span-to-thickness ratio*

The influence of the mixed boundary conditions and span-to-thickness ratio is now considered. The plate is simply supported along the edges parallel to the x-axis while the other edges have simply supported (S), clamped (C) or free (F) boundary conditions. The notation SS, SC, CC, FF, FS and FC refer to the boundary conditions of two edges parallel to the y-axis only. The three layer cross-ply $[0/90/0]$ square plate is analyzed with $E_1 = 40E_2$ and a 14×14 mesh as indicated in Fig. 3. Table 4 contains the normalized fundamental frequencies for various span-to-thickness ratios obtained by the present method and other solutions of Liew et al. [5] using MLSDQ method, RBF's results by Ferreira et al. [7] and exact solutions [14,18]. It can be seen that the accuracy of the present method compares very well with exact solutions and other numerical results.

Furthermore, the comparison of the first five natural frequencies with other methods for a clamped three-layer cross-ply $[0/90/0]$ square plate is also presented in Table 5. The first four mode shapes obtained by the present method are also depicted in Fig. 8. It is found that the present results in general indicate good agreement with other cited solutions.

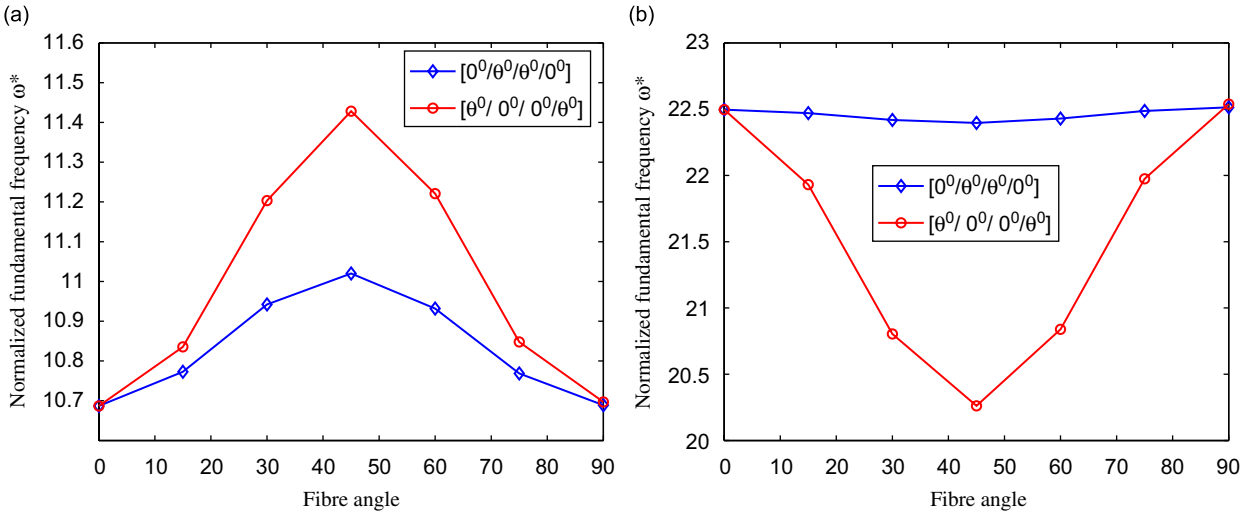

Fig. 7. Effect of fiber orientation and stacking sequence on fundamental frequencies of square laminated plates: (a) SSSS edge condition; (b) CCCC edge condition.

Table 4
Cross-ply [0/90/0] square plate with various mixed boundaries and span-to-thickness ratios: comparison of normalized fundamental frequencies with other solutions ($\omega^* = (\omega a^2/h)\sqrt{\rho/E_2}$, $E_1/E_2 = 40$)

a/h	Model	SS	SC	CC	FF	FS	FC
5	MISQ20	10.2780 (−0.117%)	10.6280 (−0.169%)	11.2387 (−0.242%)	4.0717 (0.461%)	4.5613 (0.381%)	5.9370 (0%)
	RBF [7]	10.307 (0.165%)	10.658 (0.113%)	11.274 (0.071%)	– –	– –	– –
	MLSDQ [5]	10.290 (0%)	10.647 (0.009%)	11.266 (0%)	4.054 (0.025%)	4.545 (0.022%)	5.938 (0.017%)
	Exact [18,14]	10.290	10.646	11.266	4.053	4.544	5.937
10	MISQ20	14.7823 (0.110%)	17.1806 (0.033%)	19.6614 (−0.039%)	4.3679 (0.573%)	4.9401 (0.531%)	7.3372 (0.084%)
	RBF [7]	14.804 (0.257%)	17.199 (0.139%)	19.678 (0.046%)	– –	– –	– –
	MLSDQ [5]	14.767 (0.007%)	17.176 (0.006%)	19.669 (0%)	4.343 (0%)	4.917 (0.061%)	7.333 (0.028%)
	Exact [18,14]	14.766	17.175	19.669	4.343	4.914	7.331
100	MISQ20	18.9095 (0.098%)	28.4750 (−0.091%)	40.5937 (−0.366%)	4.4835 (0.594%)	5.1007 (0.487%)	8.2665 (−0.030%)
	RBF [7]	18.355 (−2.837%)	28.165 (−1.179%)	40.234 (−1.249%)	– –	– –	– –
	MLSDQ [5]	18.769 (−0.646%)	28.164 (−1.182%)	40.004 (−1.814%)	4.439 (−0.404%)	5.301 (4.433%)	8.451 (2.201%)
	Exact [18,14]	18.891	28.501	40.743	4.457	5.076	8.269

The values in parentheses correspond to relative error percentage when compared to exact solution.

Table 5
Clamped cross-ply [0/90/0] square plate: comparison of the first five natural frequencies with other solutions

a/h	Model	Mode				
		1	2	3	4	5
5	MISQ20	4.4671	6.7365	7.7706	8.7678	9.2988
	p-Ritz [20]	4.447	6.642	7.700	9.185	9.738
	Global-local [24]	4.540	6.524	8.178	9.473	9.492
10	MISQ20	7.4542	10.5909	14.0808	16.0497	16.0868
	p-Ritz [20]	7.411	10.393	13.913	15.429	15.806
	MLSDQ [6]	7.432	10.399	13.958	15.467	15.838
	Global-local [24]	7.484	10.207	14.340	14.863	16.070
	Jian et al. [25]	7.451	10.451	13.993	15.534	15.896
20	MISQ20	11.0454	14.2988	21.4609	23.6389	25.4605
	p-Ritz [20]	10.953	14.028	20.388	23.196	24.978
	Global-local [24]	11.003	14.064	20.321	23.498	25.350
	Jian et al. [25]	11.015	14.152	20.691	23.323	25.142
100	MISQ20	14.6199	17.7013	25.5625	38.2411	39.3269
	p-Ritz [20]	14.666	17.614	24.511	35.532	39.157
	MLSDQ [6]	14.674	17.668	24.594	35.897	39.625
	Global-local [24]	14.601	17.812	25.236	37.168	38.528
	Jian et al. [25]	14.583	17.762	25.004	36.644	38.073

4.2. Skew laminated plates

This section deals with five-layer symmetric cross-ply and angle-ply skew laminated plates. Simply supported and clamped edges are considered with various skew angles α from 0° to 60°. The span-to-thickness

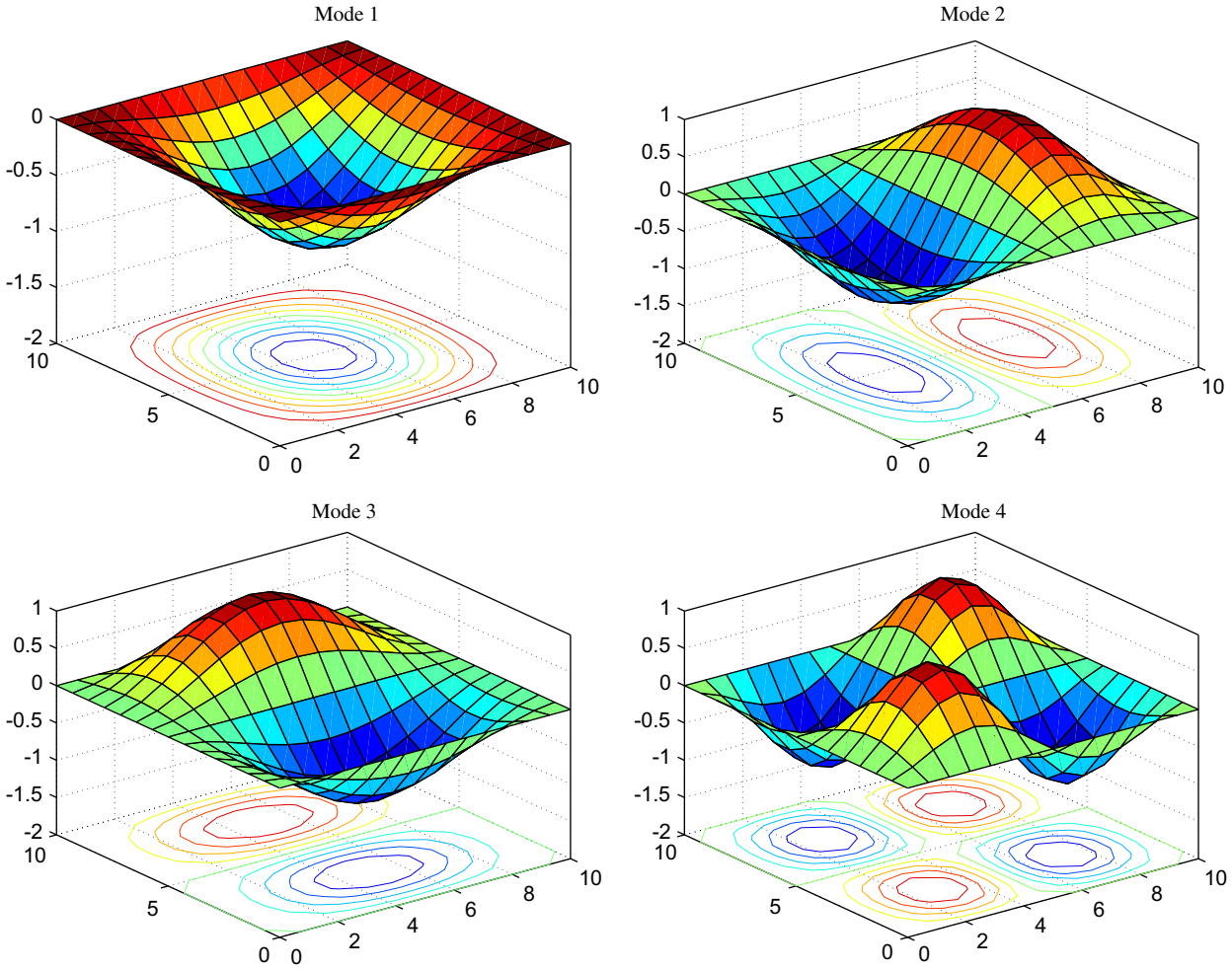

Fig. 8. Mode shapes for clamped cross-ply [0/90/0] square plate ($E_1/E_2 = 40$, $a/h = 10$).

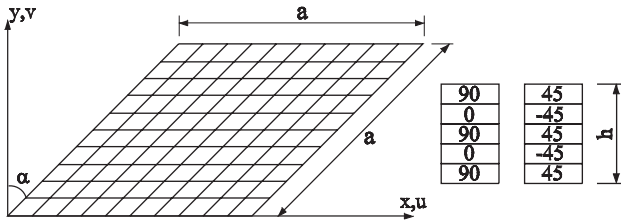

Fig. 9. Geometry and discretization of skew laminated plates.

ratio a/h is taken to be 10 and the entire plate is modeled using $6 \times 6, 10 \times 10$ and 14×14 meshes. A representative sketch of the 10×10 mesh used in the analysis is displayed in Fig. 9.

Tables 6 and 7 present the normalized fundamental frequencies of the cross-ply [90/0/90/0/90] with simply supported and clamped edges, respectively, while Tables 8 and 9 show the normalized fundamental frequencies of the angle-ply $[45/-45/45/-45/45]$ with simply supported and clamped boundaries. The results calculated using MLSDQ method by Liew et al. [5], B-spline Rayleigh–Ritz method of Wang et al. [26] and RBF of Ferreira et al. [7] are also listed for comparison. It can be seen that there is a good agreement between the present results and other existing solutions for both cases of cross-ply and angle-ply laminates.

Table 6
Simply supported cross-ply [90/0/90/0/90] skew plate with various skew angles: convergence of fundamental frequencies and comparison with other solutions ($\omega^* = (\omega a^2\sqrt{\rho/E_2})/(\pi^2 h), E_1/E_2 = 40, a/h = 10$)

Model	Mesh	α				
		0°	15°	30°	45°	60°
MISQ20	6 × 6	1.6030	1.7267	2.1441	3.0021	4.7710
	10 × 10	1.5797	1.6977	2.0963	2.9141	4.6033
	14 × 14	1.5733	1.6896	2.0820	2.8855	4.5412
MLSDQ [5]		1.5709	1.6886	2.1026	2.8798	4.4998
RBF [7]		1.5791	1.6917	2.0799	2.8228	4.3761
B-spline [26]		1.5699	–	2.0844	2.8825	–

Table 7
Clamped cross-ply [90/0/90/0/90] skew plate with various skew angles: convergence of fundamental frequencies and comparison with other solutions ($\omega^* = (\omega a^2\sqrt{\rho/E_2})/(\pi^2 h)$, $E_1/E_2 = 40$, $a/h = 10$)

Model	Mesh	α				
		0°	15°	30°	45°	60°
MISQ20	6 × 6	2.4550	2.5528	2.8901	3.6260	5.2538
	10 × 10	2.4014	2.4958	2.8194	3.5200	5.0610
	14 × 14	2.3869	2.4803	2.7998	3.4893	4.9989
MLSDQ [5]		2.3790	2.4725	2.7927	3.4723	4.9430
RBF [7]		2.4021	2.4932	2.8005	3.4923	4.9541
B-spline [26]		2.3820	–	2.7921	3.4738	–

Table 8
Simply supported angle-ply [45/ − 45/45/ − 45/45] skew plate with various skew angles: convergence of fundamental frequencies and comparison with other solutions ($\omega^* = (\omega a^2\sqrt{\rho/E_2})/(\pi^2 h)$, $E_1/E_2 = 40$, $a/h = 10$)

Model	Mesh	α				
		0°	15°	30°	45°	60°
MISQ20	6 × 6	1.8768	1.9255	2.1546	2.7185	4.1758
	10 × 10	1.8491	1.8969	2.1093	2.6286	4.0249
	14 × 14	1.8413	1.8889	2.0955	2.5672	3.9718
MLSDQ [5]		1.8248	1.8838	2.0074	2.5028	4.0227
RBF [7]		1.8357	1.8586	2.0382	2.4862	3.8619
B-spline [26]		1.8792	–	2.0002	2.4788	–

The numerical accuracy is slightly dependent on the skew angle α (accuracy deteriorates with increasing α) but insensitive to lay-up sequence. The first four mode shapes obtained by the present methods for CCCC and SSSS cases of the [90/0/90/0/90] laminated plates are also depicted in Figs. 10 and 11, respectively.

4.3. Circular laminated plates

A circular symmetric four-layer $[\theta/-\theta/-\theta/\theta]$ laminated plate with a diameter D and a thickness h as shown in Fig. 12 is analyzed. The span-to-thickness ratio a/h is taken to be 10 in the computation. Two types of boundary conditions, simply supported (SSSS) and clamped (CCCC) with various fiber orientation angles $\theta = 0^\circ, 15^\circ, 30^\circ, 45^\circ$ are considered.

Table 9
Clamped angle-ply [45/ − 45/45/ − 45/45] skew plate with various skew angles: convergence of fundamental frequencies and comparison with other solutions ($\omega^* = (\omega a^2\sqrt{\rho/E_2})/(\pi^2 h)$, $E_1/E_2 = 40$, $a/h = 10$)

Model	Mesh	α				
		0°	15°	30°	45°	60°
MISQ20	6 × 6	2.3551	2.4242	2.7566	3.5013	5.1549
	10 × 10	2.3045	2.3713	2.6892	3.3977	4.9605
	14 × 14	2.2908	2.3570	2.6708	3.3683	4.8982
MLSDQ [5]		2.2787	2.3504	2.6636	3.3594	4.8566
RBF [7]		2.3324	2.3962	2.6981	3.3747	4.8548
B-spline [26]		2.2857	–	2.6626	3.3523	–

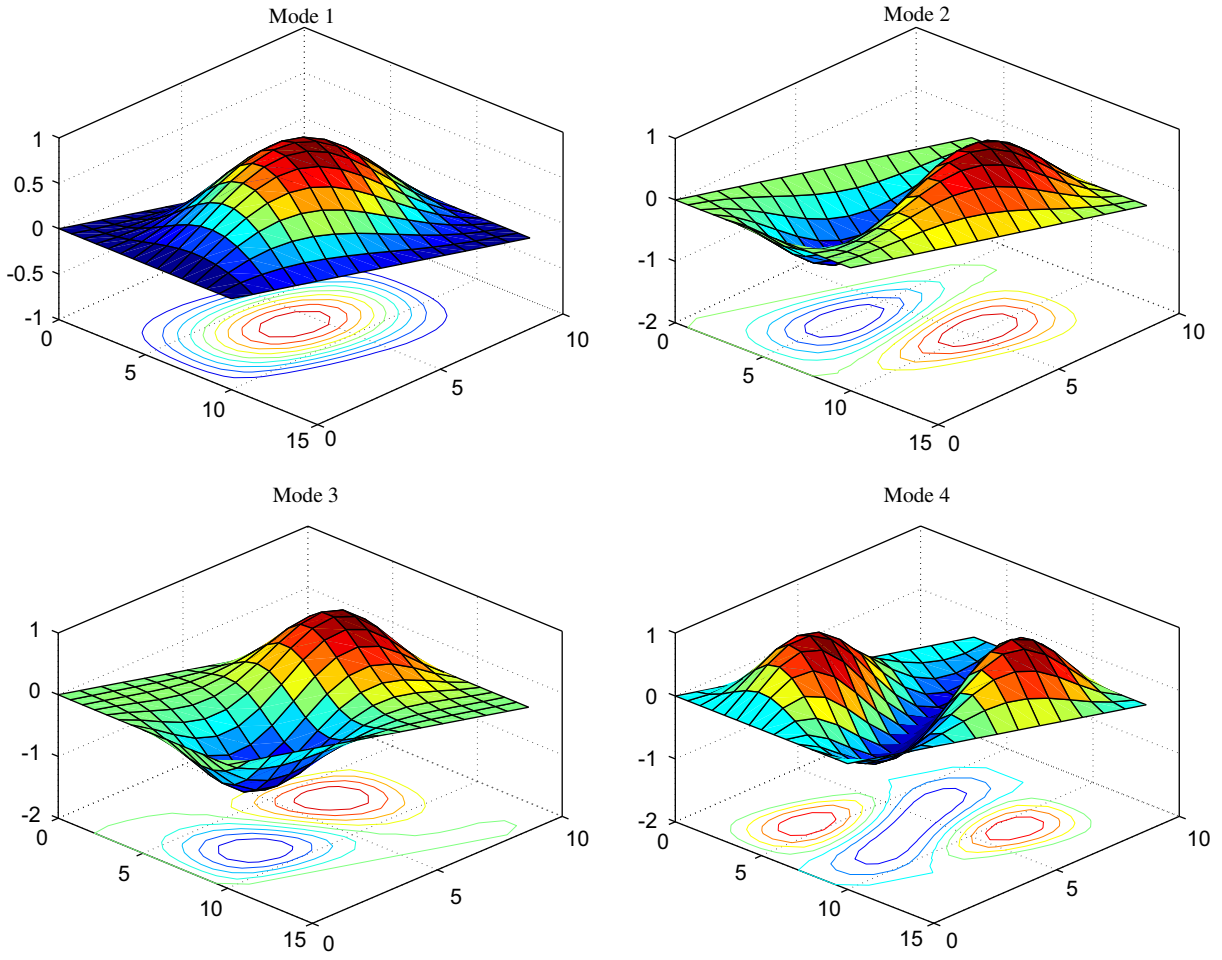

Fig. 10. Mode shapes for clamped cross-ply [90/0/90/0/90] skew plate ($\alpha = 30°$, $a/h = 10$, $E_1/E_2 = 40$).

The effect of the ply angle θ on the normalized fundamental frequency of the simply supported and clamped circular laminated plate is presented in Table 10. The natural frequencies of the first six modes in the case of clamped edge conditions are also presented in Table 11. It is observed that the numerical results obtained by the present method are comparable with Liew's results [5].

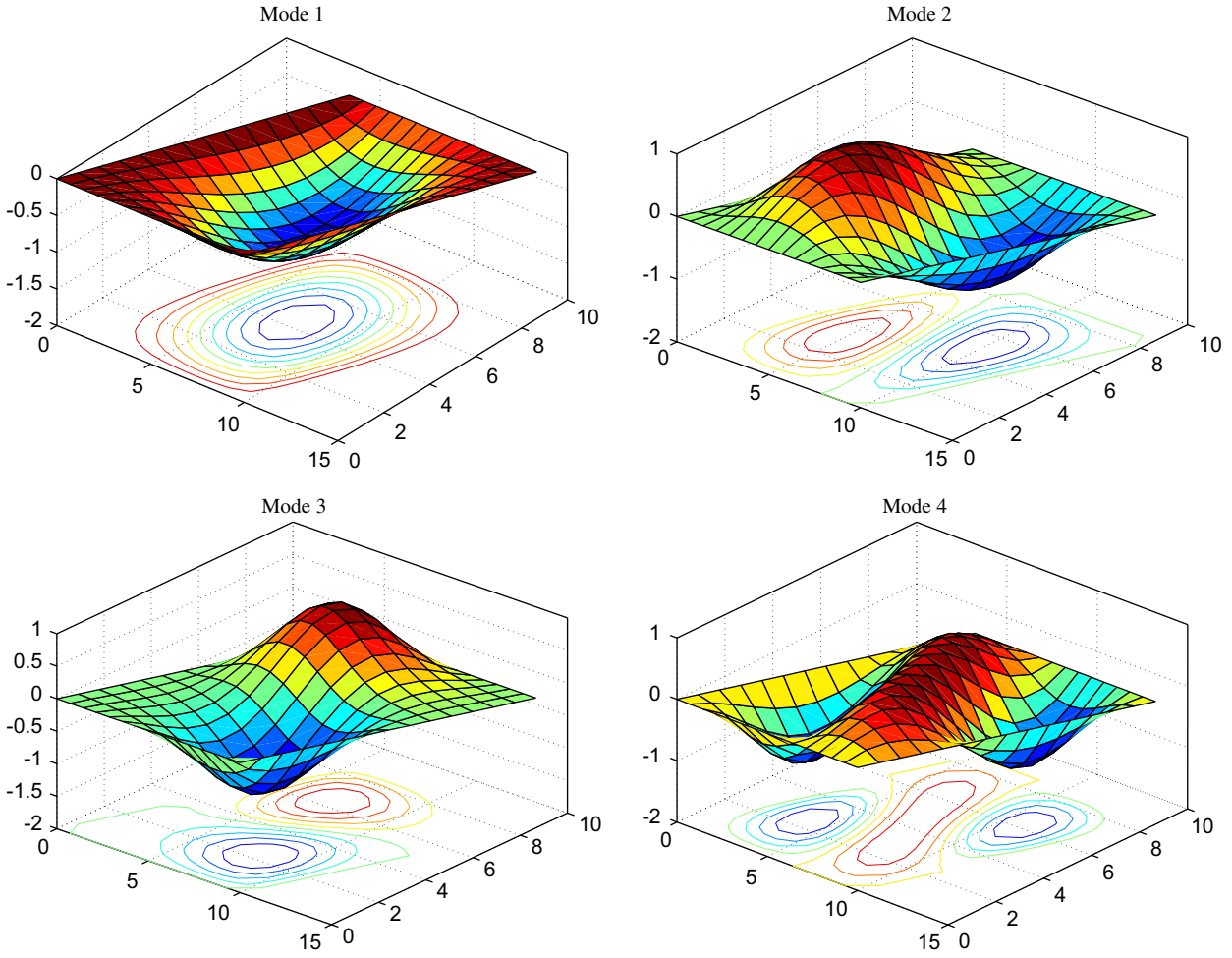

Fig. 11. Mode shapes for simply supported cross-ply [90/0/90/0/90] skew plate ($\alpha = 30^\circ$, $a/h = 10$, $E_1/E_2 = 40$).

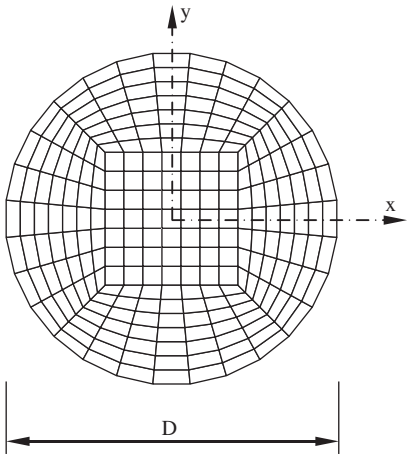

Fig. 12. Geometry and discretization of a circular laminated plate.

Table 10
Circular 4-layer $[\theta/-\theta/-\theta/\theta]$ laminated plates with various boundary conditions and ply angles: comparison of fundamental frequencies with other solutions ($\omega^* = (\omega a^2/h)\sqrt{\rho/E_2}$, $E_1/E_2 = 40, a/h = 10$)

Model	B.C	θ			
		0	15	30	45
MISQ20	SSSS	16.168	16.448	16.924	17.162
MLSDQ [5]		16.167	16.475	16.928	17.119
MISQ20	CCCC	22.123	22.698	24.046	24.766
MLSDQ [5]		22.211	22.774	24.071	24.752

Table 11
Clamped circular 4-layer $[\theta/-\theta/-\theta/\theta]$ laminated plate: comparison of the normalized natural frequencies of the first six modes ($\omega^* = (\omega a^2/h)\sqrt{\rho/E_2}$, $E_1/E_2 = 40, a/h = 10$)

θ	Model	Mode					
		1	2	3	4	5	6
0	MISQ20	22.123	29.768	41.726	42.805	50.756	56.950
	MLSDQ [5]	22.211	29.651	41.101	42.635	50.309	54.553
15	MISQ20	22.698	31.568	43.635	44.318	53.468	60.012
	MLSDQ [5]	22.774	31.455	43.350	43.469	52.872	57.386
30	MISQ20	24.046	36.399	44.189	52.028	57.478	67.099
	MLSDQ [5]	24.071	36.153	43.968	51.074	56.315	66.220
45	MISQ20	24.766	39.441	43.817	57.907	57.945	66.297
	MLSDQ [5]	24.752	39.181	43.607	56.759	56.967	65.571

4.4. Multi-layer cylindrical shells

The cross-ply laminated cylindrical panel with a radius $R = 100$ and a side length $L = 20$ subjected to simply supported boundaries is studied. The total thickness of the panel is $h = 0.2$. All layers have equal thickness and are made of the same material: $E_1/E_2 = 25$, $G_{12} = G_{13} = 0.5E_2$, $G_{23} = 0.2E_2$, $v_{12} = v_{13} = v_{23} = 0.25$, $\rho = 1$. The SCFs are assumed to be 5/6. Three kinds of lay-up sequence: [0/90], [0/90/0] and [0/90/90/0] are considered. Considering only doubly symmetric modes, a quadrant designated as ABCD as shown in Fig. 13 is modeled. The $4 \times 4, 6 \times 6$ and 8×8 meshes are used in computing the fundamental frequencies associated with the doubly symmetric modes. The convergence study of the normalized fundamental frequency is presented in Table 12. The present results are also compared with other numerical solutions such as results of Liu and To [27] using layer-wise shell element, of Jayasankar [28] using nine-node degenerated shell element and the analytical solution by Reddy [29].

It can be seen that the accuracy of the present element is compared very favorably with other elements and the method is also convergent with mesh refinement. The present element can provide accurate prediction of the solution with much reduced degrees of freedom and its performance with respect to analytical solution is excellent.

4.5. Multi-layer spherical shell

A clamped nine-layered cross-ply [0/90/0/90/0/90/0/90/0] laminated spherical panel as shown in Fig. 14 is considered. The panel has a radius $R = 10$ and a side length $a = 1$. The total thickness of the panel is $h = 0.01$. All layers are of equal thickness and same material properties: $E_1 = 2.0685 \times 10^{11}$, $E_2 = E_1/40$,

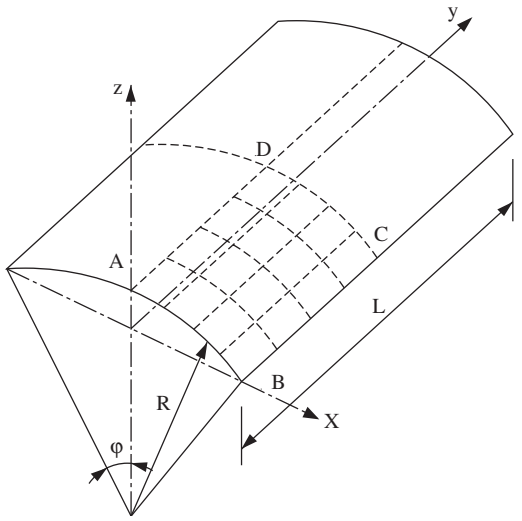

Fig. 13. Geometry and discretization of laminated cylindrical shells.

Table 12
Simply supported laminated cylindrical shells: convergence of normalized fundamental frequencies $\omega^* = (\omega L^2/h)\sqrt{\rho/E_2}$ for doubly symmetric modes and comparison with other solutions

Model	Mesh	Lay-up		
		[0/90]	[0/90/0]	[0/90/90/0]
MISQ20	4×4	17.061	20.575	20.694
	6×6	16.833	20.340	20.461
	8×8	16.736	20.240	20.367
		(0.408%)	(−0.452%)	(0.029%)
Layer-wise [27]	8×8	17.390	20.960	20.960
		(4.332%)	(3.089%)	(2.942%)
9-node shell [28]	5×5	17.7	–	–
		(6.192%)	–	–
Analytic [29]		16.668	20.332	20.361

$G_{12} = G_{13} = 0.5E_2$, $G_{23} = 0.6E_2$, $v_{12} = 0.25$ and $\rho = 1605$. The SCFs are $k_1^2 = k_2^2 = 5/6$. Three different finite element meshes are used $6 \times 6, 10 \times 10$, and 14×14 for modeling a full sphere shell.

Table 13 gives the first four normalized natural frequencies obtained by the present method in comparison with the solution of Jayasankar [28] using nine-node degenerated shell element. It can be seen that the present results agree well with the solutions given by Jayasankar.

5. Conclusions

In this paper, the MISQ20 element is further developed and successfully applied to analyze the free vibration of laminated plate/shell structures within the framework of the first-order shear deformation plate theory (FSDT). Several numerical investigations are conducted and the obtained results are in excellent agreement with other available numerical and analytic solutions. It is found that the present element is relatively simple but yields slightly better accuracy for thin to thick laminated plates/shells with various boundary conditions, modulus ratios and stacking sequences. Since the integration is done on the element

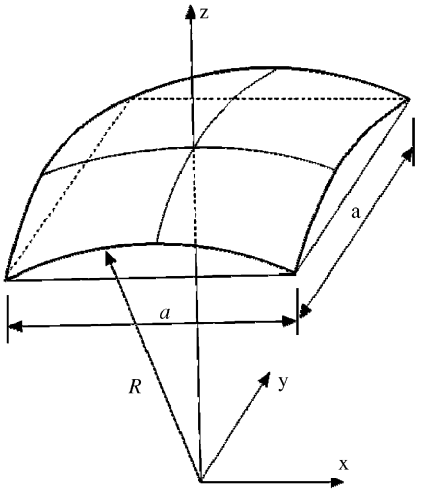

Fig. 14. Geometry data of a spherical shell.

Table 13
Clamped 9-layer $[(0/90)_2/0_s]$ cross-ply spherical shell: comparison the normalized fundamental frequencies $\omega^* = (\omega a^2/h)\sqrt{\rho/E_2}$ with other solutions

Model	Mesh	Mode 1	Mode 2	Mode 3	Mode 4
MISQ20	6×6	69.61	98.25	118.15	136.05
	10×10	67.94	88.24	104.45	119.73
	14×14	67.51	86.00	101.27	115.88
9-node shell [28]	15×15	67.43	84.16	99.71	113.70

boundaries for the bending and membrane terms, the present element remains accurate even when it is highly distorted.

Acknowledgments

The first author is supported by the Faculty of Engineering and Surveying (FoES) and the Computational Engineering and Science Research Centre (CESRC), USQ, Australia. These supports are gratefully acknowledged. We also would like to thank the referees for their helpful comments.

References

[1] C.W. Bert, Research on dynamics of composite sandwich plates, *Shock and Vibration Digest* 14 (1982) 17–34.
[2] S.Q. Mohamad, Recent research advances in the dynamic behavior of shell: 1989–2000. Part 1: laminated composite shells, *ASME Applied Mechanics Reviews* 55 (4) (2002) 325–350.
[3] H.T.Y. Yang, S. Saigal, A. Masud, R.K. Kapania, A survey of recent shell finite elements, *International Journal for Numerical Methods in Engineering* 47 (2000) 101–127.
[4] S.P. Lim, X.L. Chen, G.R. Liu, An element free Galerkin method for the free vibration analysis of composite laminates of complicated shape, *Composite Structures* 59 (2003) 279–289.
[5] K.M. Liew, Y.Q. Huang, J.N. Reddy, Vibration analysis of symmetrically laminated plates based on FSDT using the moving least squares differential quadrature method, *Computer Methods in Applied Mechanics and Engineering* 192 (2003) 2203–2222.
[6] W. Lanhe, L. Hua, W. Daobin, Vibration analysis of generally laminated composite plates by the moving least squares differential quadrature method, *Composite Structures* 68 (2005) 319–330.

[7] A.J.M. Ferreira, R.M.N. Jorge, C.M.C. Roque, Free vibration analysis of symmetric laminated composite plates by FSDT and radial basis functions, *Computer Methods in Applied Mechanics and Engineering* 194 (2005) 4265–4278.
[8] A.J.M. Ferreira, G.E. Fasshauer, Analysis of natural frequencies of composite plates by an RBF-pseudospectral method, *Composite Structures* 79 (2) (2007) 202–210.
[9] J. Wang, K.M. Liew, M.J. Tan, S. Rajendran, Analysis of rectangular laminated composite plates via FSDT meshless method, *International Journal of Mechanical Sciences* 44 (2002) 1275–1293.
[10] G.R. Liu, K.Y. Dai, T.T. Nguyen, A smoothed finite element method for mechanics problems, *Computational Mechanics* 39 (6) (2007) 859–877.
[11] G.R. Liu, T.T. Nguyen, K.Y. Dai, K.Y. Lam, Theoretical aspects of the smoothed finite element method (SFEM), *International Journal for Numerical Methods in Engineering* 71 (8) (2006) 902–930.
[12] H. Nguyen-Van, N. Mai-Duy, T. Tran-Cong, A simple and accurate four-node quadrilateral element using stabilized nodal integration for laminated plates, *CMC: Computers, Materials and Continua* 6 (3) (2007) 159–175.
[13] E.N. Dvorkin, K.J. Bathe, A four node plate bending element based on Mindlin-Reissner plate theory and a mixed interpolation, *International Journal for Numerical Methods in Engineering* 21 (1985) 367–383.
[14] J.N. Reddy, *Mechanics of Laminated Composite Plates and Shells—Theory and Analysis*, CRC Press, Boca Raton, FL, 2004.
[15] S. Valchoutsis, Shear correction factors for plates and shells, *International Journal for Numerical Methods in Engineering* 33 (1992) 1537–1552.
[16] S.V. Kulkarni, S.N. Chatterjee, Shear correction factors for laminated plates, *AIAA Journal* 17 (1979) 498–499.
[17] J.M. Whitney, Shear correction factors for orthotropic laminates under static load, *Journal of Applied Mechanics* 40 (1973) 302–304.
[18] A.A. Khdeir, L. Librescu, Analysis of symmetric cross-ply elastic plates using a higher-order theory. Part II: buckling and free vibration, *Composite Structures* 9 (1988) 259–277.
[19] J.N. Reddy, P.H. Phan, Stability and vibration of isotropic, orthotropic and laminated plates according to a higher order shear deformation theory, *Journal of Sound and Vibration* 98 (1985) 157–170.
[20] K.M. Liew, Solving the vibration of thick symmetric laminates by Reissner/Mindlin plate theory and the p-Ritz method, *Journal of Sound and Vibration* 198 (3) (1996) 343–360.
[21] C.P. Wu, W.Y. Chen, Vibration and stability of laminated plates based on a local higher-order plate theory, *Journal of Sound and Vibration* 177 (4) (1994) 503–520.
[22] H. Matsunaga, Vibration and stability of cross-ply laminated composite plates according to a global higher-order plate theory, *Composite Structures* 48 (2000) 231–244.
[23] A.G. Striz, K.N. Cho, C.W. Bert, Free vibration of laminated rectangular plates analyzed by higher-order individual-layer theory, *Journal of Sound and Vibration* 145 (1991) 429–442.
[24] W. Zhen, C. Wanji, Free vibration of laminated composite and sandwich plates using global-local higher-order theory, *Journal of Sound and Vibration* 298 (2006) 333–349.
[25] W.S. Jian, N. Akihiro, K. Hiroshi, Vibration analysis of fully clamped arbitrary laminated plate, *Composite Structures* 63 (2004) 115–122.
[26] S. Wang, Free vibration analysis of skew fiber-reinforced composite laminates based on first-order shear deformation plate theory, *Computer and Structures* 63 (1997) 525–538.
[27] M.L. Liu, C.W.S. To, Free vibration analysis of laminated composite shell structures using hybrid strain based layerwise finite elements, *Finite Elements in Analysis and Design* 40 (2003) 83–120.
[28] S. Jayasankar, S. Mahesh, S. Narayanan, C. Padmanabhan, Dynamic analysis of layered composite shells using nine node degenerate shell elements, *Journal of Sound and Vibration* 299 (2007) 1–11.
[29] J.N. Reddy, Exact solutions of moderately thick laminated shells, *ASCE Journal of Engineering Mechanics* 110 (4) (1984) 794–809.